Solution processed large area fabrication of Ag patterns as electrodes for flexible heaters, electrochromics and organic solar cells

Gupta, Ritu; Walia, Sunil; Hösel, Markus; Jensen, Jacob; Angmo, Dechan; Krebs, Frederik C; Kulkarni, Giridhar U.

Published in:
Journal of Materials Chemistry A

Link to article, DOI:
10.1039/C4TA00301B

Publication date:
2014

Journal of Materials Chemistry A

Accepted Manuscript

This article can be cited before page numbers have been issued, to do this please use: R. Gupta, S. Walia, M. Hösel, J. Jensen, D. Angmo, F. C. Krebs and G. U. Kulkarni, *J. Mater. Chem. A*, 2014, DOI: 10.1039/C4TA00301B.

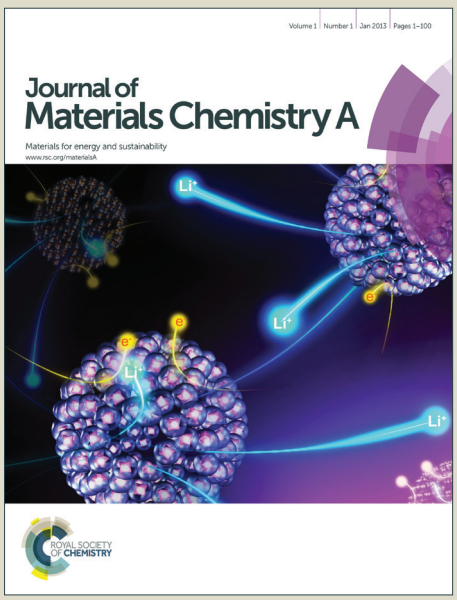

ROYAL SOCIETY OF CHEMISTRY

www.rsc.org/materialsA

View Article Online
DOI: 10.1039/C4TA00301B

Journal of Material Chemistry A RSCPublishing

ARTICLE

Solution processed large area fabrication of Ag patterns as electrodes for flexible heaters, electrochromics and organic solar cells

Cite this: DOI: 10.1039/xoxxoooooox

Ritu Gupta,[a] Sunil Walia,[a] Markus Hösel,[b] Jacob Jensen,[b] Dechan Angmo[b] Frederik C. Krebs[b]* and Giridhar U. Kulkarni[a]*

Received ooth January 2014,
Accepted ooth January 2014

DOI: 10.1039/xoxxoooooox

www.rsc.org/

A simple method for producing patterned Ag electrodes on transparent and flexible substrates is reported. The process makes use of laser printed toner as a sacrificial template for an organic precursor, which upon thermolysis and toner lift off produced highly conducting Ag electrodes. Thus, the process takes only a few minutes without any expensive instrumentation. The electrodes exhibited excellent adhesion and mechanical properties, important for flexible device application. Using Ag patterned electrodes, heaters operating at low voltages, pixelated electrochromic displays as well as organic solar cells have been demonstrated. The method is extendable to produce defect-free patterns over large areas as demonstrated by roll coating.

Introduction

Technological advancements in flexible and transparent electronics are taking place at a very fast rate.[1,2] The new generation devices – a RC circuit,[3] RFIDs,[4] sensors,[5] displays,[6] electrochromic windows,[7,8] transparent heaters,[9] transistors,[10] solar cells,[11] all rely on flexible printed functionalities distinctly different from the rigid and planar Si technology. The light weight, durability and foldability offered by flexible electronics not only bring in personal comfort but also make devices affordable much like the use-and-dispose commodity items.[12]

Flexible electronics and printing technology go hand in hand as the latter has many ready solutions to offer. Currently used techniques such as photolithography,[13] soft lithography[14] and nanoimprint lithography[15] may be capable of large area patterning, but the preparation of a suitable mask is a difficult step. Thus, large area printing with high throughput at optimum resolution is challenging. However, as the design and feature size of printed electrodes depend on the type of application, one need not always resort to high-end lithography techniques. For mass printing purposes, roll-to-roll flexography,[16] screen printing[17] and inkjet printing[18-20] have been employed with resolution down to few microns.[21] However, these techniques require expensive instrumentation. A more serious challenge arise in fabrication of top metal electrodes for organic devices, as these techniques render metal features to be quite thick (~500 nm to 2 nm) with high surface roughness, which increase the risk of electrical shorting in devices.[22]

The rapid prototyping of devices need electrodes to be printed like daily printable paper at one's disposal. In this context, xerographic printing using commercially available printers has gained importance. In the past, the xerographic toner patterns from ordinary printers have been utilized for making photomasks for photolithography and masters for elastomeric stamps in soft lithography.[23] The toner patterns printed on conductive substrates have been utilized as etch resist mask.[24] It has also been utilized for low cost patterning and rapid prototyping of microfluidic devices.[25,26] The printed toner patterns have been used in combination with a conducting polymer to create line patterns for fabricating interconnects in a push button array.[27] Toner-Metal patterns have been prepared for the fabrication of DNA chips.[28] A short review on fabrication of devices using commercial laser printers is provided in ESI†, Table S1. We have developed a novel and simple, solution-processed method for the fabrication of metallic line patterns where the printed toner acts as a sacrificial template for a metal precursor, which is retained in designated patterns after toner lift-off using common solvents. Using commonly available laser printer, we have been able to print electrodes on large area polyethylene terephthalate (PET) sheets and fabricate several prototype devices such as semi-transparent heaters, addressable electrochromic devices as well as organic solar cells. The possibility of adopting the method for roll-to-roll processing towards fabrication of devices is also demonstrated.

Results and discussion

Fabrication and characterization

The conducting electrodes are fabricated on a transparent, flexible PET substrate following the procedure illustrated in Fig. 1a. Briefly, the CAD drawing is printed using the standard toner supplied with the laser printer. The printed area of PET is cut into the desired size and coated with Ag precursor by spin, rod or slot-die coating depending on the area to be patterned. Different Ag inks (particle and non-particle based) were first

View Article Online
DOI: 10.1039/C4TA00301B

Journal of Material Chemistry A RSCPublishing

ARTICLE

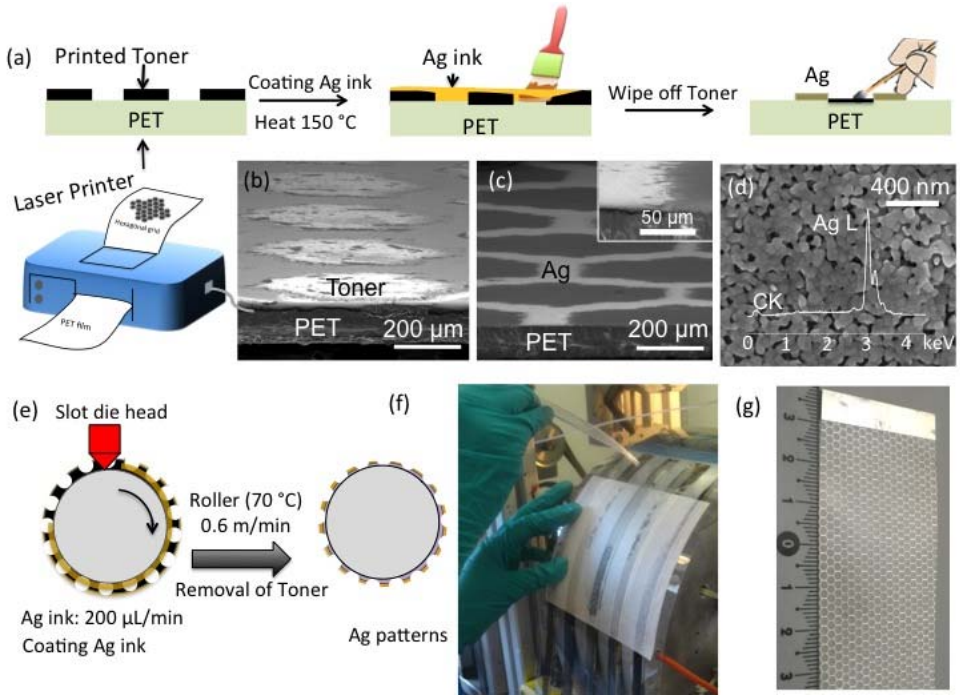

Fig. 1 Fabrication of solution processed large area Ag patterned electrodes (a) Schematic demonstrating the fabrication procedure. Tilted SEM image of the cross-sectional view of (b) toner pattern on PET substrate and (c) after developing with Ag. Inset shows the zoom in view of the cross-section of Ag printed on PET. (d) SEM image and overlapped EDS of printed Ag. (e) Ag ink coating on toner printed PET sheets using slot die head roll coater (f) after partial metallization followed by removal of toner (g) a large area printed hexagonal Ag pattern.

tested for patterning by this technique (ESI†, Fig. S1). Typically, 100 µL of Ag precursor was spread over a 5 × 5 cm^2 area and spin coated at a rate of 1000 rpm. The Ag ink covers the whole substrate, open spaces as well as toner covered area. The Ag ink decomposes to Ag metal on heating at 150 °C within few seconds (~ 30 s), which is later developed by wetting the Ag coated toner with toluene and wiping it off with a cotton swab (Fig. 1a). The lift-off done this way is more economical than washing or sonicating in the solvent. The time is optimized to be ~30 s, above that the removal of toner becomes difficult. While below 30 s, Ag also gets washed away along with the toner and do not adhere to the substrate. After removing the toner, it was held at 150 °C for 10 min to further get rid of left-over carbon and anneal the particles (see thermogravimetric and X-ray diffraction analysis in ESI†, Fig. S2) resulting in a highly conducting Ag film with sheet resistance of ~0.12 Ω/sq (ESI†, Fig. S3). As can be seen from the SEM tilt images in Fig. 1b and c, the lift-off is neat, which is a crucial step in patterning. The optical profilometry images before and after the toner lift-off, are shown in ESI†, Fig. S4. The cross-section image in the inset shows thin Ag layer on the substrate with no trace of the toner. The printed pattern consists of interconnected Ag nanoparticles with only little carbon impurity (see overlaid EDS data). The method could be easily extended to a variety of flexible substrates by adhering them to PET, making acceptable to the printer. Substrates such as thermal tape, mica, paper, scotch tape, kapton sheet proved successful (Fig. S4). The printing method could also be extended to large area coating processes using a roll coater[29] with a slot-die head (Fig. 1e and f).The process steps involved in roll coating is same as shown in schematic in Fig. 1a. The laser printed sheets of A4 size with hexagonal patterned grids as negative images were joined together to form 1 m length (see Fig. S6). Thus formed extended sheet was mounted on a motorized roll of 300 mm diameter and the Ag precursor was dispensed at a flow rate of 200 µL/min. The schematic shows how the ink is delivered to the patterned toner printed sheet while the drum is rotated. The roller was set to 70 °C while coating at a speed of 0.6 m/min. After coating, the temperature was risen to 150 °C for 10 min to completely metallize the Ag patterns. As shown in Fig. 1f, the toner was removed by wetting it with toluene and wiping off with lint-free tissue paper. This process resulted in a neatly printed Ag patterns (see Fig. 1g) over 1 m length without any residues from toner. The ability of continuous process and the patterned area are neither limited by the laser printer nor by the processing steps and thus the

Journal Name

View Article Online
DOI: 10.1039/C4TA00301B ARTICLE

technique can be extended for roll-to-roll production as well. The Ag patterns fabricated by roll coating were further adopted for solar cell integration.

With CAD program, one may draw any arbitrary design (Fig. 2a). Printed designs of Ag involving different line widths and curvatures can be obtained on PET as shown in the photograph in Fig. 2a. The process appears quite versatile. An optical microscopic image of an Ag line from a hexagonal pattern (original design shown in the inset) shows the metal filled line with irregular edges due to pixelization effect and toner spreading (Fig. 2b). The Ag lines of varying line widths (100 - 500 μm) were printed and the resistance was measured to determine the optimum width for printing the features.

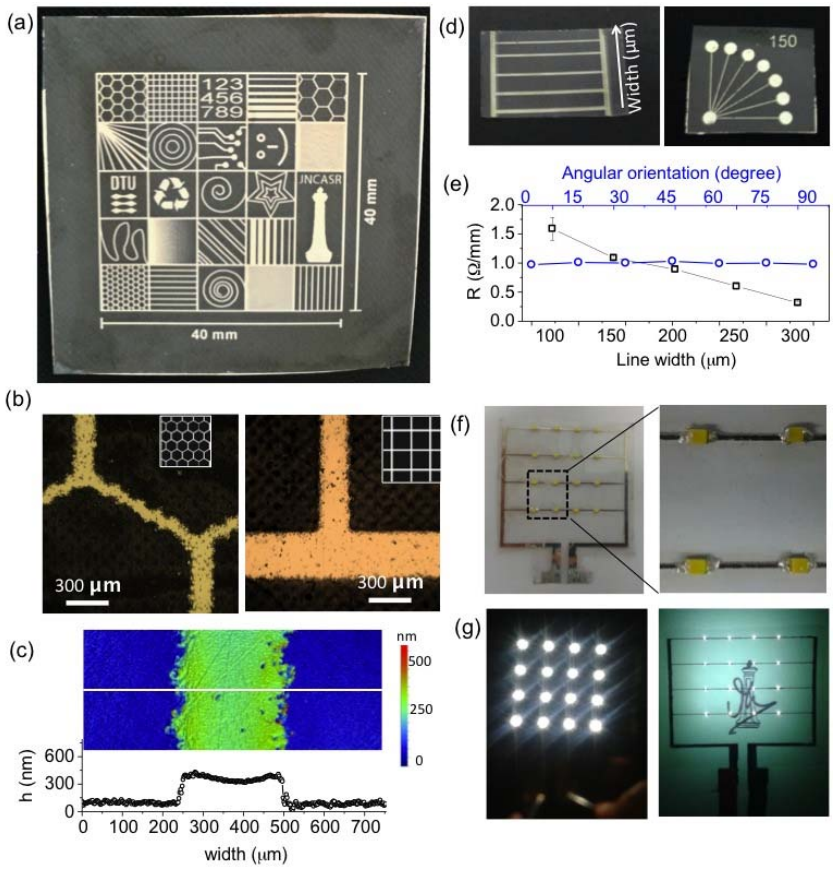

Fig. 2 (a) Different geometries and design patterns of Ag on PET. (b) Optical microscope images of the toner printed patterns (designs shown in insets). (c) Optical profilometry image of the Ag line along with the height profile. (d) Photographs of the PET substrates patterned with Ag of different line widths (left) and different angular orientation for line width of 150 μm (e) resistance values of the features shown in (d). (f) Photograph showing an array of 16 LEDs (SMD-603, white, 0.8 × 1.2 mm^2) mounted on the Ag printed gap electrodes. (g) Front view of the LED panel (left) and LED panel (viewed from back) illuminating JNCASR logo (right).

Fig. 2c shows the optical profiler 2D image of the Ag line with width of 250 μm and thickness 250 nm. As seen from the height profile, the patterned line is little thicker at the edges, but on the whole, the surface profile is smooth (roughness of ~ 5 nm), important for device applications. When the pattern is curved, the printed electrode may suffer from artifacts arising out of the digital nature of the technique well known as the staircase effect. The resistance was measured at different angular orientation for different line widths as shown in Fig. 2d. The minimum line width required for patterning while maintaining electrical continuity was 150 μm, which was later, adopted for some applications involving complex structures. The straight Ag lines are highly conducting with resistance varying between 0.2 to 2 Ω/mm for different line widths as shown in Fig. 2e (right). To demonstrate the continuity of the conducting Ag lines over large area, we assembled a 4 × 4 array of LEDs between the pre-defined gap electrodes as shown in Fig. 2f. When the voltage (12 V) was applied, all LEDs lighted up implying the electrode array was devoid of printing related defects. Interestingly, when the LED panel was held facing a picture, it produced uniform illumination and the electrode lines were nearly unnoticeable (Fig. 2g). Such panels could be used in front-lit display applications as well.

Mechanical stability of Ag electrodes

The adhesion of the printed pattern was tested by the scotch tape peeling method using an automated system (ASTM D3330). The scotch tape was peeled at 90° with a load of 0.6 - 0.8 N to the substrate. The effect of peel-off on the resistance across the electrodes is very small as seen by the multimeter readings in Fig. 3a, implying that the printed Ag has excellent adhesion on PET. The durability of the electrodes against extreme mechanical stress is evident from various tests such as rolling, bending, folding and twisting of the electrode (see Fig. 3b) performed with the maximum possible force applied playfully by an unbiased volunteer. The

View Article Online
DOI: 10.1039/C4TA00301B
Materials Horizon

flexibility test was carried out by bending the printed electrode to different radii of curvature. The resistance of the electrode remained relatively constant as seen from Fig. 3c. Upto 5000 initial cycles, the fluctuation in resistance is observed probably due to mechanical annealing of particles, which deserves a separate study. After the settling, the Ag electrodes showed excellent bending fatigue strength towards successive tension and compression cycles carried out for 50,000 times, without undergoing any failure (Fig. 3d).

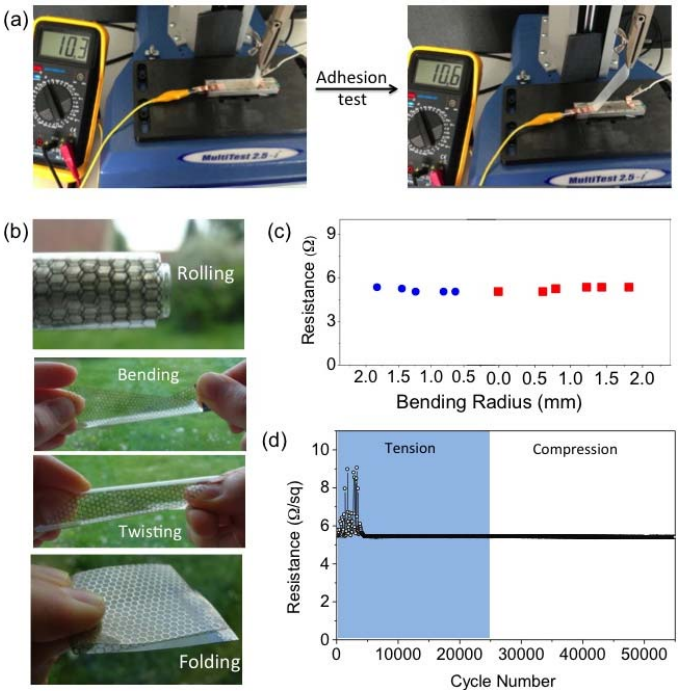

Fig. 3 Mechanical properties of Ag grid electrode (a) Adhesion test (b) The robustness of the electrode demonstrated by subjecting the electrode to rolling, bending, twisting and folding tests. (c) change in resistance with bending radius.(d) variation in R_S of the Ag grid electrode during tension and compression cycles (bending radius, 4 mm).

A semi-transparent flexible heater

As the patterning could be extended to large areas, heaters can be designed for defrosting window panels used in advertisement boards, road sign displays, thermochromic windows and teller machine front panels.[30,31] The Ag line patterns can serve as well-defined resistive heating element over a defined area. As the Ag fill factor is kept small (< 50%), it is effectively a semi-transparent heater for select applications.

An example of heater with Ag line pattern is shown in Fig. 4a. The representative thermal images taken at 0.4 and 0.8 V in Fig. 4b and c show nearly uniform temperature distribution in the middle region with average temperature of 40.9±1 °C and 78.1±4 °C, respectively. The histogram corresponding to the temperature distribution across the central area is shown in ESI†, Fig. S7. As seen from Fig. 4d, regardless of the applied voltage, the increase in temperature was fast and nearly steady state temperatures were reached in less than 60 s (see ESI†, Movie-1). As PET is thermally insulating (thermal conductivity, ~ 0.2 $W.m^{-1}K^{-1}$) which is much lower compared to Ag metal (~ 406 $W.m^{-1}K^{-1}$), the heat was confined within the patterned region. The input power required to raise the temperature was also small; for the example shown, a power of 0.4 W/cm^2 was sufficient to raise the temperature to 85 °C (Fig. 4e).The resistance decreased marginally (~3.6%) on heating around 125 °C due to annealing of particles (see ESI†, Table S2). A variety of designs (square mesh, checkers, spirals, zig-zag patterns) were tested as possible geometries for heaters (see Fig. 4f and ESI†, Fig. S8). The application of the obtained Ag line pattern as semi-transparent heater is demonstrated in the form of a defrosting window in ESI†, Fig. S9. Compared to previous reports (see ESI†, Table S2) this method provides an improved semi-transparent heater that can be operated at low voltages (0-1 V) capable of reaching relatively high temperatures (50-100 °C) with fast response (> 30 s) due to good electrical and thermal conductivity along with high mechanical strength

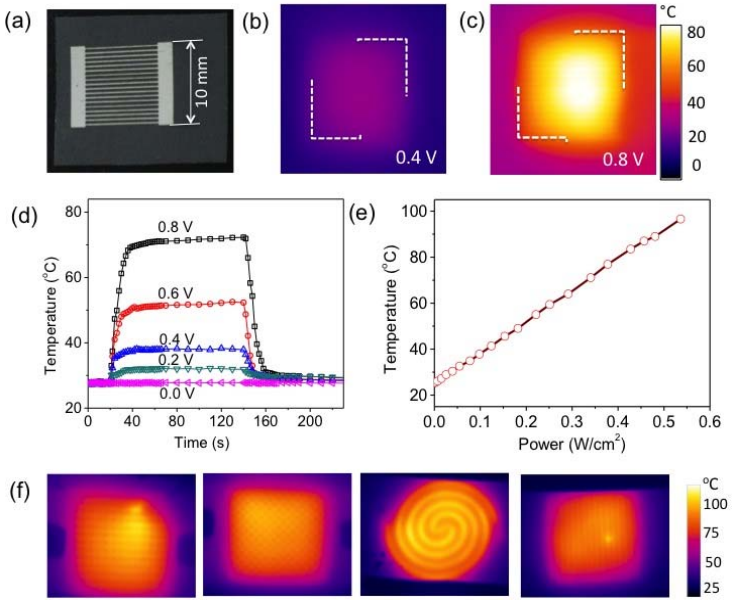

Fig. 4 (a) Photograph of Ag line pattern on PET (10 mm × 10 mm). Thermal images of the patterned electrode obtained during joule heating with bias voltages of (b) 0.4 V and (c) 0.8 V. (d) The temperature rise curve with respect to time for different applied voltages (e) rise in temperature with applied power. (f) Thermal images for various heater designs such as square mesh, pyramid shape, spiral and zig-zag path.

View Article Online
DOI: 10.1039/C4TA00301B

Journal of Material Chemistry A RSCPublishing

ARTICLE

Addressable matrix-type electrodes for electrochromic device

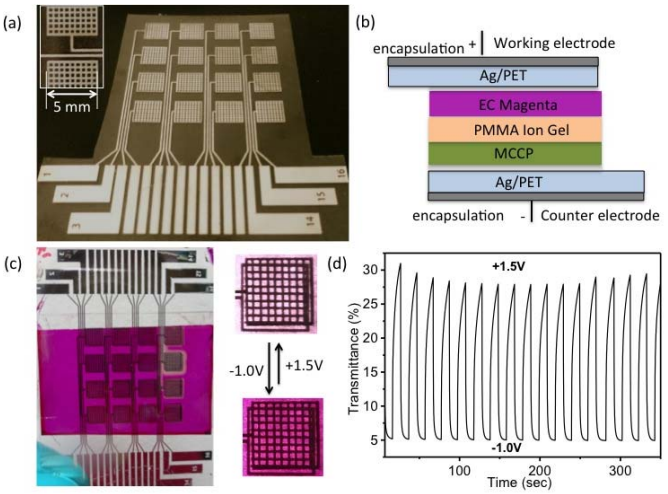

Fig. 5 An addressable electrode system with 4 × 4 pixels (each pixel is 5 × 5 mm^2) (b) electrochromic device (ECD) structure (c) Both top and bottom electrode consists of 4 × 4 pixelated regions where each pixel is defined by a square grid of Ag lines (see inset). The assembled device and its corresponding electrochromic switching at a chosen pixel. (d) variation in transmittance during switching cycles.

The versatility of the patterning technique was also used in the fabrication of pixelated electrochromic devices (ECDs) that has recently gained importance.[32] A 4 × 4 pixelated grid was fabricated using Ag electrodes as shown in Fig. 5a. The pixel size was 5 × 5 mm^2 and the pixels were interconnected by an addressable circuit. The device was fabricated by spincoating polymer solutions onto the addressable Ag grid electrodes. Two well characterized electrochromic polymers were employed, namely ECP-Magenta[33] and MCCP[34] (see Experimental) as these have been shown to work well in ECDs with optical contrasts in the range, 43% to 61%, depending on the setting.[33,34] The devices were assembled with a layered structure as depicted in Fig. 5b. The ECDs using Ag/PET electrodes could be switched at +1.5 and -1.0 V, with a transmittance (corrected for substrate and encapsulant absorption) of ~ 42% in the reduced state and ~ 64% in the oxidized state with a response time of ~ 10 seconds (Fig. 5d and ESI†, Fig. S10). Although the contrast is somewhat lower (~ 22%), the method presented demonstrates the possibility of making addressable matrix displays.

Current collecting grid electrode for Organic Solar Cells

The transparent conducting films such as ITO, PEDOT:PSS, graphene and CNT mesh have been combined with metal grid as current collecting electrode to improve the conductivity and charge collection efficiency of solar cells.[35,36] There is a great deal of literature on different methods adopted for the fabrication of grids at low cost and high throughput (see ESI†, Table S3). Most printing methods produce electrodes with high roughness leading to shorting between the electrodes.[37-40] In our case, the topography of the printed Ag is relatively smooth (see Fig. 2f), the transmittance and sheet resistance of the pattern can be easily adjusted by varying the width and the spacing (see ESI†, Fig. S11). The hexagonal Ag grid (150 µm width and 2 mm spacing) is highly conducting with an overall sheet resistance of 4 Ω/sq and transmittance of 82% (Fig. 6a).The empty voids in the Ag grid seen clearly in Fig. 6b (top) are filled by conducting PEDOT:PSS to create a hybrid transparent conducting electrode (Fig. 6b, bottom). The transmission spectra of the Ag grid, Ag/PEDOT:PSS hybrid and PEDOT:PSS are shown in Fig. 6c. Fig. 6d represents the inverted geometry of organic P3HT:PCBM solar cell employed for large area fabrication. 1 m long 3 stripes were printed in ambient conditions following the processing steps illustrated in Fig. S12 and ESI†, Table S4. The entire process resulted in printing of 200 solar cells (1 × 1 cm^2 each) in less than 2 hrs (Fig. 6e). Laser beam induced current (LBIC) mapping technique was used to characterize the different regions of the solar cell.[42] The high performance of the solar cell is clearly evident from the LBIC map which shows uniform photocurrent in almost all the areas of the cell except the shadow losses from the grid electrode (Fig. 6f). The active cell area was calculated from the LBIC image and used for converting the I-V to J-V curve. As seen from the J-V characteristics (see Fig. 6g), the solar cell configured with this grid electrode exhibited increased efficiency (1.85%) as compared to PEDOT:PSS (~ 0.6%) due to significant reduction in series resistance because of highly conducting nature of the Ag grids. A total of 12 cells were measured and the maximum value corresponding to different grid size and PEDOT based electrodes is summarized in Table 1.

Table 1 A brief summary of the solar cell performance with different grid size including PEDOT without grid for comparison.

Ag Grid (Width/Spacing)	**Grid 1+PEDOT** (150 µm/ 1 mm)	**Grid 2+PEDOT** (150 µm/ 2 mm)	**Grid 3+PEDOT** (150 µm/ 3 mm)	**PEDOT** No grid
PCE (%)	1.36	1.85	1.03	0.55
J_{SC} (mA/cm^2)	-4.85	-7.22	-6.098	-3.505
V_{oc} (V)	0.528	0.5308	0.472	0.497
FF (%)	53.05	48.475	36.056	31.735
R_{SH} (Ω/cm^2)	1421.78	1504.72	401.60	208.64
R_S (Ω/cm^2)	12.46	15.72	22.67	75.64

The EQE measurements in the wavelength range from 300 to 700 nm (Fig. 6h), show much higher values for cells prepared with Ag grid and PEDOT:PSS, compared to PEDOT:PSS alone, being consistent with higher short circuit currents (see Table 1). Thus, efficient solar cells could be prepared by incorporating Ag grids as current collector in PEDOT:PSS based organic solar cells. The results obtained in this study, albeit the simplicity of the fabrication process, are indeed comparable to those in the literature pertaining to Ag grid/PEDOT:PSS hybrid electrodes (see ESI†, Table S3).

View Article Online
DOI: 10.1039/C4TA00301B

Journal of Material Chemistry A RSCPublishing

ARTICLE

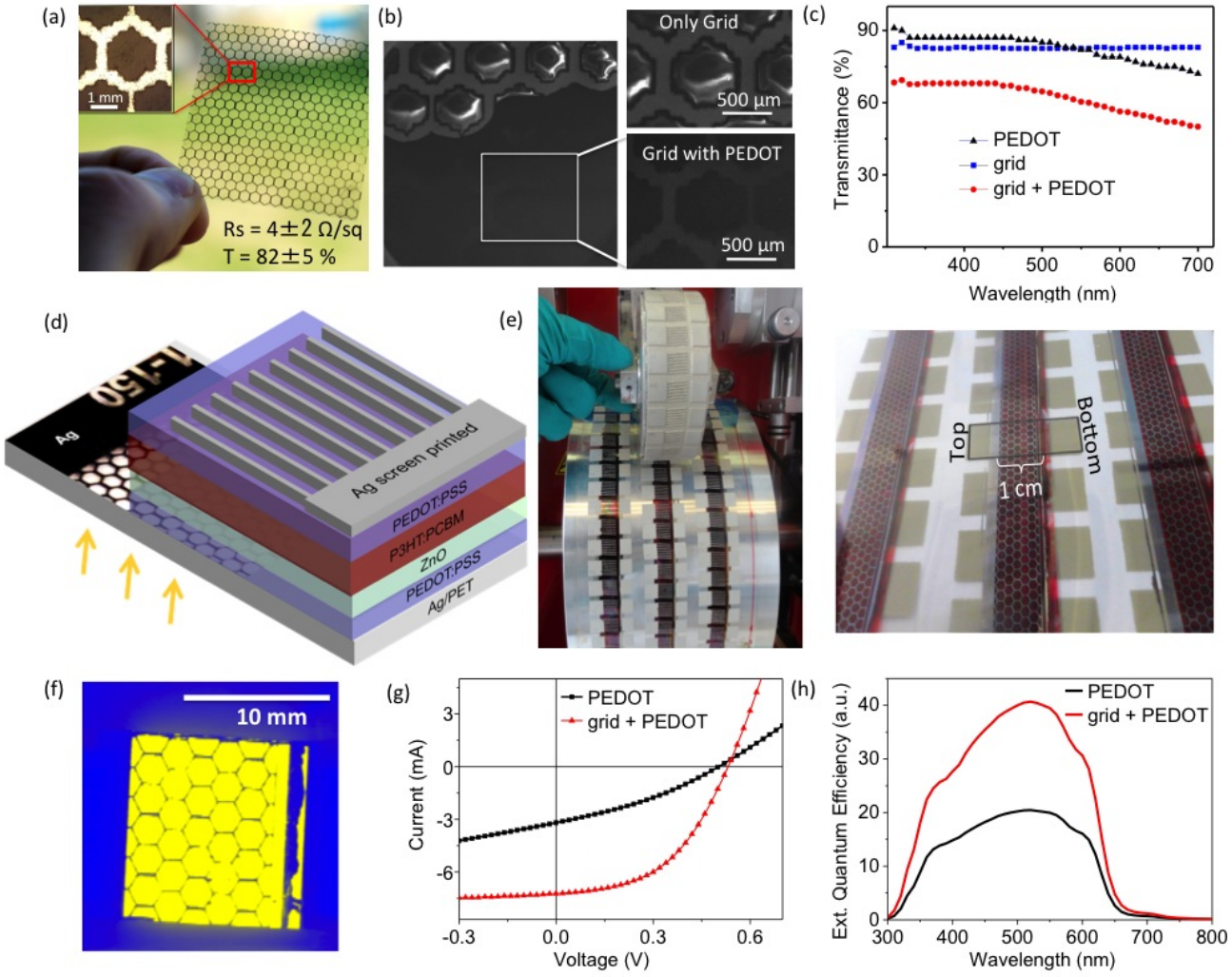

Fig. 6 (a) Hexagonal current collecting Ag grid with line width of 150 µm and spacing of 2 mm (b) SEM image of the Ag grid coated with PEDOT:PSS (c) Transmission spectra of the PEDOT:PSS coated Ag grid compared with bare Ag grid and PEDOT:PSS film. (d) Schematic showing the solar cell geometry (e) the roll coater with a mounted flexo-printing roller displaying the fabricated solar cells with an enlarged view on the right. (f) Laser Beam Induced Current (LBIC) map of a solar cell grid electrode (g) I-V characteristics and (h) external quantum efficiencies of the solar cells fabricated with Ag grid-PEDOT:PSS hybrid electrode and only PEDOT:PSS for comparison.

Conclusions

Using a common laser printer, a Ag precursor ink and common solvents, we have developed a method of patterning Ag electrodes on flexible and transparent substrates. Besides being simple, the method is adoptable to computer graphics to produce various electrode designs on printer friendly sheets such as PET, kapton, tape, mica etc. The Ag precursor ink could be easily metallized on hot plate or oven leading to highly conducting electrodes of different shapes and sizes as specified in the design. The electrodes possessed excellent mechanical flexibility and adhesion properties too. The versatility of the method was demonstrated by fabricating transparent flexible heaters, an addressable electrochromic device and organic solar cells. With low applied voltages (< 2 V), the heaters could reach 120 ºC (what PET can sustain) and showed excellent temperature uniformity over cm^2 regions. With addressable and pixelated Ag electrodes, an electrochromic device was fabricated which was able to switch between magenta and colorless states at low voltages with reasonable response time. By adopting the method to roll coating, large area electrode patterns as well as solar active organic layers could be assembled under ambient conditions and the fabricated cells exhibited efficiency of up to 1.8%. The above examples clearly demonstrate the versatile nature of the method developed in this study, which can be easily implemented in any common work place such as a cottage industry.

Journal Name View Article Online DOI: 10.1039/C4TA00501B ARTICLE

Experimental

Fabrication of Ag Grid Electrodes

The patterns were designed using Adobe Illustrator software (CS6 version) and printed on 150 µm thick PET (Melinex ST-506, DuPont) using a Ricoh Aficio C5000 laser printer with a printing resolution of 600 dpi (b/w mode). The Melinex sheets possess the desired mechanical, thermal and adhesion properties. The particle-free Ag precursor ink (Inktec PR010) used in this study is purchased from Inktec, Korea. Other non-particle Ag ink from Kunshan Hisense (SC-100) and a nanoparticle-based Ag ink from PARU (PR010) were also tried out in initial tests.

Characterization

The optical microscope (Laben, India) is used for measuring the features size. Surface profilometry was carried out using a contactless, 3D, white light interferometer (Veeco Wyko NT9100). SEM imaging was done using Nova NanoSEM 600 instrument (FEI Co., The Netherlands). The transmittance of the film is measured in specular and diffuse mode using Perkin–Elmer Lambda 900 UV/visible/near-IR spectrophotometer with integrated sphere. In case of Ag grids, the transmittance spectra were measured from 3 different areas with an optical beam size of 5 × 2 mm^2 and the average profile was plotted. Sheet resistance is measured using 4-Point Probe Station (Jandel Model RM3, London). The adhesion test was carried out using scotch tape and flexibility testing was done using Mechmesin Multi test 2.5i unit to pull the scotch tape perpendicular to the substrate.

Inverted Solar Cell Fabrication

The patterned Ag/PET was cleaned gently with IPA and treated under oxygen plasma for 5 min to generate the hydrophilic surface. A PEDOT:PSS (Clevios PH1000) was spin coated on Ag grid at 1200 rpm resulting in a thin layer of 50 nm. The electron transport layer of ZnO nanoparticle solution in acetone was spin coated at 1000 rpm and heated for at least 3 min at 120 °C. The preparation of ZnO nanoparticles is reported previously in literature.[42] The P3HT and PCBM were dissolved in 1,2- dichlorobenzene (1:1 w/w, 20 mg/mL) to obtain P3HT:PCBM solution for active layer coating. The P3HT:PCBM solution was spin-coated on PET/Ag/PEDOT:PSS/ZnO substrates at 1000 rpm. PEDOT:PSS (Agfa 5010) was diluted 2:1 (w/w) with isopropanol and then spin coated onto the active layer to form the hole transport layer. The substrates were heated at 130 °C for 3 min. Finally, Ag paste (DuPont PV410) was screen printed onto the spin-coated films to form the positive electrode. Finally, all the devices were annealed for 5 min to cure the Ag layer and encapsulated with DELO LP655 uv-curable adhesive before characterization. All the measurements were carried out at ambient conditions under AM 1.5G illumination. The EQE was measured using a solar cell spectral response measurement system from PV Instruments, Inc. (Model QEX10).

Fabrication of flexible heater

Different designs like straight line, interpenetrated spiral and zig-zag lines were made with Ag for transparent heaters. The electrode contacts were established using thick epoxy Ag paint. The substrate was mounted for imaging with supports at both ends such that the patterned area is kept hanging in air while the imaging is done from the back side of the patterned area. The voltage was applied using Keithley-2400 and thermal imaging was carried out using Testo thermal imager (Testo-885).The images were analysed using offline software.

Fabrication of Electrochromic device

The Ag printed grid electrodes were UV/ozone treated for 60 min prior to spincoating of electrochromic polymers and electrolyte gel. The polymers were synthesized according to literature and toluene solutions (20mg/mL) of poly((2,2-bis(2-ethylhexyloxymethyl)-propylene-1,3-dioxy)-3,4-thiophene-2,5-diyl, (ECP-magenta) and poly(N-octadecyl-(propylene-1,3-dioxy)-3,4-pyrrole-2,5-diyl), (MCCP) was spin coated at 800 rpm on the primary and secondary electrodes respectively.[32] This electrolyte gel comprising of poly(methylmethacrylate) (PMMA) and 1-ethyl-2-methyl-imidazolium-bis(triflouromethanesulfonyl)imide was spin coated at 1500 rpm on both electrodes. The device was finally assembled by placing the two electrodes against each other and encapsulating with an adhesive foil from 3M.

LBIC measurement

The LBIC experiment was carried out using a high speed system developed at Risø, DTU (Denmark).[41] It is a custom made setup with 410 nm laser diode (5 mW output power, 100 µm spot size ~ 65 W/cm^2, Thorlabs) mounted on a computer controlled XY-stage. A custom written computer program was used to scan the solar cell devices in a raster pattern in 200 µm steps in the X and the Y directions, logging the coordinates and measuring the current. The results were then converted to yellow/blue colored bitmaps in 255 different hues with another custom written program. Bright yellow represents the highest absolute current extracted while blue represents the lowest current.

Acknowledgements

RG, GUK and SW thank Prof. C N R Rao for being constant source of inspiration. RG thanks Swati (JNCASR) for assistance. The financial support from DST, India for EU-Indian framework of the Large cells project (FP7/2007-2013, grant no. 261936) is gratefully acknowledged.

Notes and references

[a] Ritu Gupta, Sunil Walia, Prof. Giridhar. U. Kulkarni [*], Chemistry and Physics of Materials Unit, DST Unit on Nanoscience, Jawaharlal Nehru Centre for Advanced Scientific Research, Jakkur P.O., Bangalore, India-560064, Email: kulkarni@jncasr.ac.in

[b]Markus Hösel, Jacob Jensen and Dechan Angmo, Prof. Frederik C. Krebs [*], Department of Energy Conversion and Storage, Technical University of Denmark, Frederiksborgvej 399, DK-4000 Roskilde, Denmark, Email: frkr@dtu.dk

†Electronic Supplementary Information (ESI) available: [Table S1: literature on usage of commercial laser printers, Fig. S 1 Different Ag ink types used for testing Fig.S2: Thermogravimetric analysis of Ag precursor ink and XRD pattern of Ag ink before and after heating, Fig. S3: Temperature dependent resistivity of Ag, Fig. S4: Optical profilometry image of Toner/PET and Ag PET after developing with Ag and removal of toner, Fig. S5: Ag pattern printed on various substrates, Fig. S6: Printing of large area A4 size patterns for roll coater, Fig. S7: Histograms showing the average temperature distribution across the sample area corresponding to thermal images acquired for the line heater in Figure 4 at 0.4 V and 0.8 V, Table S2: Change in resistance after heating cycles at different voltages. Fig. S8: Photographs of Various heater designs, Table S3: A brief survey of literature transparent micro-heaters, Fig. S9: Defrosting window is demonstrated using the zig-zag patterned Ag electrode, Fig. S10: Transmission spectrum from the substrate and the encapsulant, Fig. S11: Ag grids as transparent conducting electrode. Table S4: A brief literature survey of hybrid Ag grid current collecting electrode and PEDOT, Table S5: The optimized conditions for roll coating of solar cells, Fig. S12: Photographs

View Article Online
DOI: 10.1039/C4TA00301B

demonstrating the sequential steps for fabrication of solar cell.]. See DOI: 10.1039/b000000x/

References

1. J. A. Rogers, Z. Bao, K. Baldwin, A. Dodabalapur, B. Crone, V. R. Raju, V. Kuck, H. Katz, K. Amundson, J. Ewing, P. Drzaic, *Proc. Natl. Acad. Sci. U.S.A.*, 2001, **98**, 4835.
2. R. Parashkov, E. Becker, T. Riedl, H. H. Johannes, W. Kowalsky, *Proc. IEEE.,* 2005, **93**, 1321.
3. N. Kurra, D. Dutta, G. U. Kulkarni, *Phys. Chem. Chem. Phys.*, 2013, **15**, 8367.
4. N. Komoda, M. Nogi, K. Suganuma, K. Kohno, Y. Akiyama, K. Otsuka, *Nanoscale*, 2012, **4**, 3148.
5. B. Radha, A. A. Sagade, G. U. Kulkarni, *ACS Appl. Mater. Interfaces*, 2011, **3**, 2173.
6. A. Sandström, H. F. Dam, F. C. Krebs, L. Edman, Nat. Commun.2012, **3**, 1002.
7. R. J. Mortimer, A. L. Dyer, J. R. Reynolds, *Displays*, 2006, **27**, 2.
8. J. Jensen, H. F. Dam, J. R. Reynolds, A. L. Dyer, F. C. Krebs, *J. Polym. Sci. Part B: Polym. Phys.*, 2012, **50**, 536.
9. J. Kang, H. Kim, K. S. Kim, S.-K. Lee, S. Bae, J.-H. Ahn, Y.-J. Kim, J. B. Choi, B. H. Hong, *Nano lett*., 2011, **11**, 5154.
10. K. Nomura, H. Ohta, A. Takagi, T. Kamiya, M. Hirano, H. Hosono, *Nature*, 2004, **432**, 488.
11. P. Sommer-Larsen, M. Jørgensen, R. R. Søndergaard, M. Hösel, F. C. Krebs, *Energy Technology*, 2013, **1**, 15.
12. S. R. Forrest, *Nature*, 2004, **428**, 911.
13. J. D. Ryckman, Y. Jiao, S. M. Weiss, *Sci. Rep*., 2013, **3**.
14. K. Tvingstedt, O. Inganäs, *Adv. Mater.*, 2007, **19**, 2893.
15. M.-G. Kang, M.-S. Kim, J. Kim, L. J. Guo, *Adv. Mater.,* 2008, **20**, 4408.
16. M. Hösel, F. C. Krebs, *J. Mater. Chem.*, 2012, **22**, 15683.
17. B. Winther-Jensen, F. C. Krebs, *Sol. Energy Mater. Sol. Cells*, 2006, **90**, 123.
18. Y.-I. Lee, S. Kim, K.-J. Lee, N. V. Myung, Y.-H. Choa, *Thin Solid Films,* 2013, **536**, 160.
19. D. Angmo, T. T. Larsen-Olsen, M. Jørgensen, R. R. Søndergaard, F. C. Krebs, *Adv. Energy Mater*., 2012, **3**, 172.
20. J. S. Kang, H. S. Kim, J. Ryu, H. Thomas Hahn, S. Jang, J. W. Joung, *J Mater Sci: Mater Electron*, 2010, **21**, 1213.
21. J.-S. Yu, I. Kim, J.-S. Kim, J. Jo, T. T. Larsen-Olsen, R. R. Søndergaard, M. Hösel, D. Angmo, M. Jørgensen, F. C. Krebs, *Nanoscale*, 2012, **4**, 6032.
22. T. Aernouts, P. Vanlaeke, W. Geens, J. Poortmans, P. Heremans, S. Borghs, R. Mertens, R. Andriessen, L. Leenders, *Thin Solid Films,* 2004, **22**, 451-452.
23. H. Hwang, G. Kang, J. H. Yeon, Y. Nam, J.-K. Park, *Lab Chip*, 2009, **9**, 167.
24. M. Abdelgawad, A. R. Wheeler, *Adv. Mater*., 2007, **19**, 133.
25. M. Abdelgawad, M. W. L. Watson, E. W. K. Young, J. M. Mudrik, M. D. Ungrin, A. R. Wheeler, *Lab Chip*, 2008, **8**, 1379.
26. W. K. T. Coltro, D. P. de Jesus, J. A. F. da Silva, C. L. do Lago, E. Carrilho, *Electrophoresis,* 2010, **31**, 2487.
27. D. Hohnholz, H. Okuzaki, A. G. MacDiarmid, *Adv. Funct. Mater*., 2005, **15**, 51.
28. A. R. Liberski, J. T. Delaney, A. Liberska, J. Perelaer, M. Schwarz, T. Schüler, R. Möller, U. S. Schubert, *RSC Adv*., 2012, **2**, 2308.
29. J. E. Carlé, T. R. Andersen, M. Helgesen, E. Bundgaard, M. Jørgensen, F. C. Krebs, *Sol. Energy Mater. Sol. Cells*, 2013, **108**, 126.
30. H.-S. Jang, S. K. Jeon, S. H. Nahm, *Carbon*, 2011, 49, 111.
31. C. Celle, C. Mayousse, E. Moreau, H. Basti, A. Carella, J. P. Simonato, *Nano Res*., 2012, **5**, 427.
32. J. Kawahara, P. Andersson Ersman, D. Nilsson, K. Katoh, Y. Nakata, M. Sandberg, M. Nilsson, G. Gustafsson, M. Berggren, *J. Polym. Sci. Part B: Polym. Phys*., 2013, **51**, 265.
33. B. D. Reeves, C. R. G. Grenier, A. A. Argun, A. Cirpan, T. D. McCarley, J. R. Reynolds, *Macromolecules*, 2004, **37**, 7559.
34. E. P. Knott, M. R. Craig, D. Y. Liu, J. E. Babiarz, A. L. Dyer, J. R. Reynolds, *J. Mater. Chem*., 2012, **22**, 4953.
35. Y. Zhu, Z. Sun, Z. Yan, Z. Jin, J. M. Tour, *ACS Nano*, 2011, **5**, 6472.
36. Q. Zhang, X. Wan, F. Xing, L. Huang, G. Long, N. Yi, W. Ni, Z. Liu, J. Tian, Y. Chen, *Nano Res*., 2013, **6**, 478.
37. Y. Li, L. Mao, Y. Gao, P. Zhang, C. Li, C. Ma, Y. Tu, Z. Cui, L. Chen, *Sol. Energy Mater. Sol. Cells*, 2013, **113**, 85.
38. Y. Galagan, E. W. C. Coenen, S. Sabik, H. H. Gorter, M. Barink, S. C. Veenstra, J. M. Kroon, R. Andriessen, P. W. M. Blom, *Sol. Energy Mater. Sol. Cells*, 2012, **104**, 32.
39. Y. Galagan, J. E. J. M. Rubingh, R. Andriessen, C. C. Fan, P. W. M. Blom, S. C. Veenstra, J. M. Kroon, *Sol. Energy Mater. Sol. Cells*, 2011, **95**, 1339.
40. Y. Galagan, B. Zimmermann, E. W. C. Coenen, M. Jørgensen, D. M. Tanenbaum, F. C. Krebs, H. Gorter, S. Sabik, L. H. Slooff, S. C. Veenstra, J. M. Kroon, R. Andriessen, *Adv. Energy Mater*., 2012, **2**, 103.
41. F. C. Krebs, R. Søndergaard, M. Jørgensen, *Sol. Energy Mater. Sol. Cells*, 2011, **95**, 1348.
42. F. C. Krebs, Y. Thomann, R. Thomann, J. W. Andreasen, *Nanotechnology*, 2008, **19**, 424013.

View Article Online
DOI: 10.1039/C4TA00301B

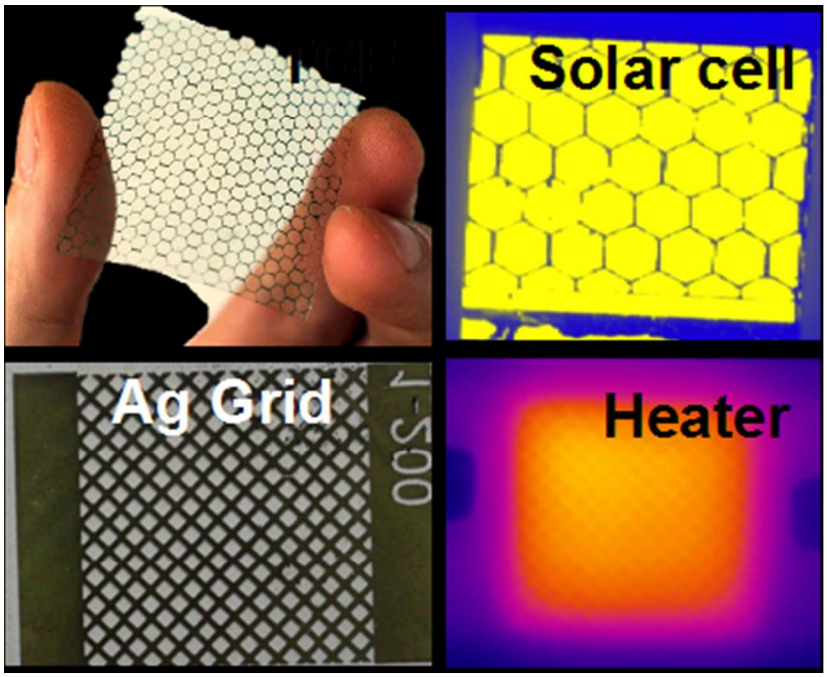

129x112mm (80 x 75 DPI)